Volume 22
Number 35
21 September 2020
Pages 19379–20144

PCCP

Physical Chemistry Chemical Physics

rsc.li/pccp

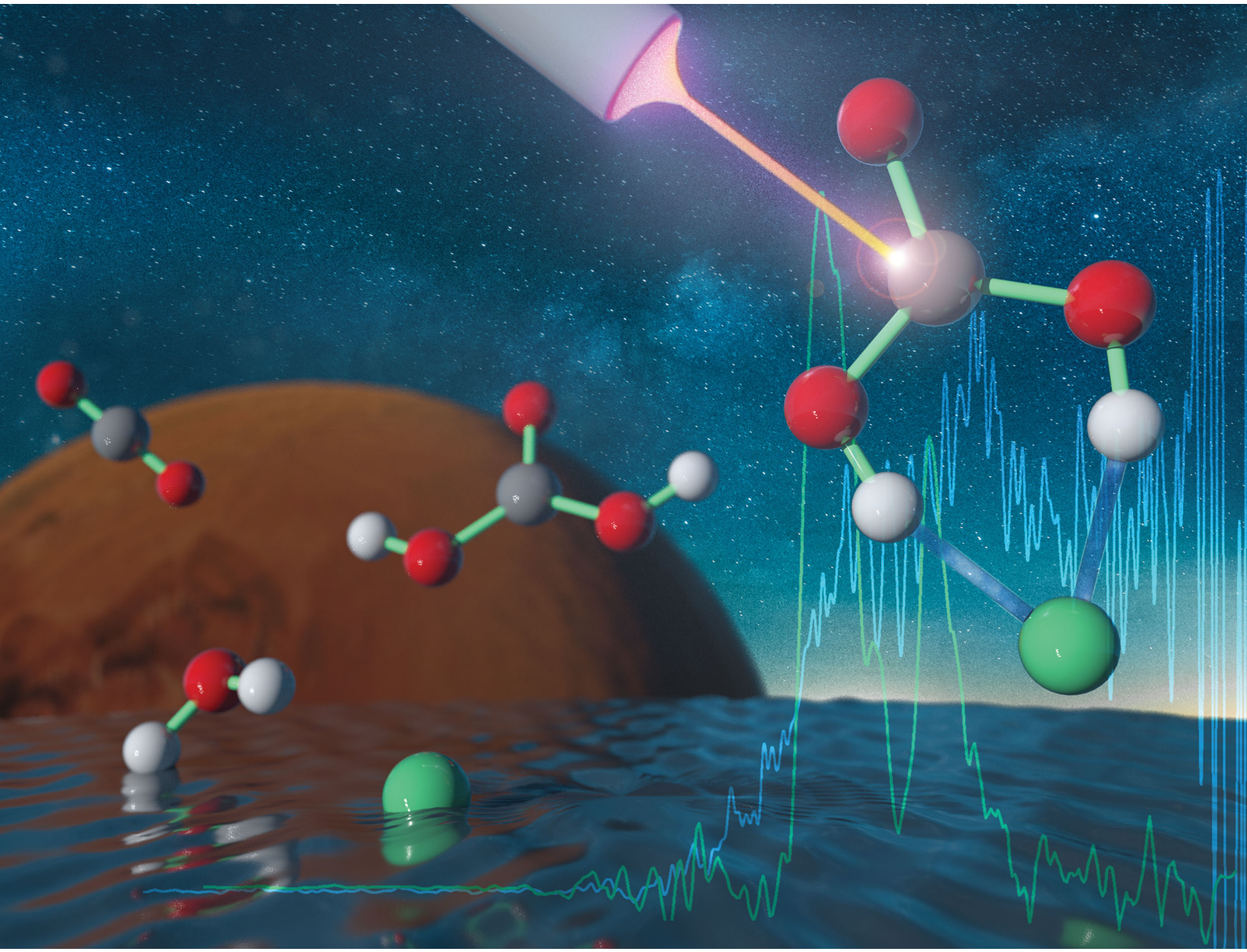

ISSN 1463-9076

ROYAL SOCIETY OF CHEMISTRY

PAPER

Xiaoguo Zhou, Xue-Bin Wang *et al.*
Spectroscopic evidence for intact carbonic acid stabilized by halide anions in the gas phase

PCCP

ROYAL SOCIETY OF CHEMISTRY

PAPER

View Article Online
View Journal | View Issue

Cite this: *Phys. Chem. Chem. Phys.*, 2020, **22**, 19459

Spectroscopic evidence for intact carbonic acid stabilized by halide anions in the gas phase†

Hanhui Zhang,[a] Wenjin Cao,[b] Qinqin Yuan,[b] Lei Wang,[a] Xiaoguo Zhou,*[a] Shilin Liu[a] and Xue-Bin Wang*[b]

Received 30th April 2020,
Accepted 12th June 2020

DOI: 10.1039/d0cp02338h

rsc.li/pccp

This work shows elusive carbonic acid being effectively stabilized in the gas phase by interacting with halide anions X^- (X = F, Cl, Br, and I). The formed $H_2CO_3{\cdot}X^-$ complexes, characterized by negative ion photoelectron spectroscopy and *ab initio* calculations, all contain intact *trans–trans* carbonic acid binding onto the respective halide *via* two identical strong ionic O–H···X^- hydrogen bonds. For X = Cl, Br, and I, the complex spectra exhibit the corresponding X^- signature by simply shifting to the higher binding energy side, while an extremely 2 eV wide broader band is observed for X = F. This spectroscopic evidence indicates that an excess electron is removed from each halide in the former case, while a proton is transferred from carbonic acid to fluoride upon electron detachment for the latter. The above $H_2CO_3{\cdot}X^-$ structures as well as those of the previously studied $H_2SO_4{\cdot}X^-$ along the homologous halogen series cannot be explained using the proton affinity (PA) argument. Instead, a qualitative correlation is found between these structural motifs and the constituent acid pK_a values, strongly suggesting that pK_a is a more suitable factor to predict correct acid–base chemistry between these diprotic oxyacids and halides.

Introduction

Carbonic acid is a diprotic oxyacid of fundamental interest in geography,[1,2] astrophysics,[3–5] biochemistry[6,7] and other related fields. It not only contributes to ocean acidification and affects organic matter and nutrients,[1] but it also serves as a prospective interstellar molecule on the Martian surface, comets and icy grains.[3–5] Moreover, it plays vital physiological roles in the H_2CO_3/HCO_3^- buffer system that stabilizes the blood pH and other biological fluids,[6] maintaining a large flux of protons that sustain metabolic life-supporting processes and rapid enzymatic reactions.[7] Therefore, the molecular conformation of carbonic acid-containing complexes, especially those involving strong hydrogen bonding, is crucial to understanding their related chemical reactivities.

For a long time, carbonic acid has generally been considered to be thermodynamically unstable, undergoing dissociation to carbon dioxide and water in the gas phase. Although a potential well was suggested by theoretical calculations for isolated carbonic acid,[8] the catalyzations by various ambient species, like solvents, surfaces or other constituents in solution, can efficiently lower the barrier.[9–11] In 1987, Schwarz and coworkers performed the first direct detection of the gas-phase H_2CO_3 molecule in mass spectra of heated ammonium bicarbonate (NH_4HCO_3) vapor.[12] The first spectroscopic measurement was done in 2009 using Fourier-transform microwave spectroscopy, in which the gaseous *cis–trans* H_2CO_3 molecule was produced by passing a pulsed electric discharge of carbon dioxide under supersonic expansion conditions through a water reservoir.[13] In addition, a debate has proceeded for more than 20 years on the two polymorphs of solid carbonic acid, α- and β-H_2CO_3.[14–21] Despite a lot of spectral characterization reported for both of them,[22–24] Reisenauer *et al.* verified that α-H_2CO_3 actually belongs to the carbonic acid monomethyl ester, while the β polymorph is true H_2CO_3.[25]

Compared with its gas and solid phases, aqueous carbonic acid is relatively more complicated. The deuterated carbonic acid yielded by the ultrafast protonation of bicarbonate in deuterium oxide solution was reported to have a limited lifetime of 300 nanoseconds.[26] Such a fleeting lifetime implies that hydrogen bonding interaction between carbonic acid and Lewis bases like water might be central to its related chemical

[a] *Hefei National Laboratory for Physical Sciences at the Microscale, Department of Chemical Physics, University of Science and Technology of China, Hefei, Anhui 230026, P. R. China. E-mail: xzhou@ustc.edu.cn*
[b] *Physical Sciences Division, Pacific Northwest National Laboratory, 902 Battelle Boulevard, P. O. Box 999, MS K8-88, Richland, Washington 99352, USA. E-mail: xuebin.wang@pnnl.gov*

† Electronic supplementary information (ESI) available: Optimized structures of the *trans–trans* neutral radicals (Fig. S1), electron density topological graphs (Fig. S2), NPA charge distributions (Fig. S3), schematic structures of all isomers of $H_2CO_3{\cdot}F^-$ and their neutrals (Fig. S4), Frank–Condon simulated spectra for different isomers of $H_2CO_3{\cdot}F^-$ (Fig. S5), binding energies of carbonic acid and halides (Table S1), topological properties of $H_2CO_3{\cdot}X^-$ (Table S2), and relative energies and enthalpies of formation of $H_2CO_3{\cdot}X^-$ in Isomer 1 conformation (Table S3). See DOI: 10.1039/d0cp02338h

processes instead of carbonic acid itself. A recent investigation[7] also confirmed that in spite of its instability, carbonic acid could still serve as an effective protonating agent by matching its pK_a value, which has been accurately determined over the full physiological temperature range, perfectly accounting for its vital biological function. Though some progress has been made, there is a lack of investigations of the interactions between carbonic acid and more Lewis bases beyond water. Of particular interest are anions of high Lewis basicity such as halide anions, whose hydrogen bonding structures between carbonic acid and the ligands can provide detailed insights into the stabilization and chemistry of carbonic acid in solutions. Very recently, Thomas *et al.* measured the infrared action spectrum of the carbonic acid–fluoride complex anion in helium nanodroplets.[27] A strong ionic double hydrogen bond was proven to be the core for the remarkable stability of $F^-(H_2CO_3)$ with carbonic acid in a *trans–trans* conformation. Unfortunately, no other halide complex anions were observed in their experiments, preventing a systematic understanding of halide induced stabilization of carbonic acid over the whole series.

Notably, the fluoride anion always formed distinct hydrogen bonds compared to the other halides because it has the smallest ionic radius and highest Lewis basicity, which leads to unique local solvation structures in protic solvents, such as $F^-(H_2O)_2$[28,29] and $H_2SO_4{\cdot}F^-$.[30] Although proton affinity (PA) is usually thought as the determinant factor for a hydrogen bonding structure between the proton donor and the acceptor, this criterion fails in $H_2SO_4{\cdot}X^-$ (X = Cl, Br, I)[30] and a few other molecular clusters.[31–36] Thus, a comprehensive investigation of all halide–H_2CO_3 complexes is necessary to find the true determinant factor for hydrogen bonding structures at a molecular level, since the PA values span a wide range in the F, Cl, Br, I sequence. In addition, the halides–water and halides–carbon dioxide complexes have been investigated,[28,37,38] along with HCO_3^- dissolved in water molecule clusters,[39] providing requisite fundamental knowledge for the in-depth understanding of carbonic acid–halide interactions.

Experimental and theoretical methodologies

Negative ion photoelectron spectroscopy (NIPES)

The NIPE spectra were recorded using a low-temperature, magnetic-bottle time-of-flight (TOF) photoelectron spectrometer, coupled with an electrospray ionization source and a temperature-controlled cryogenic ion trap.[40] The $H_2CO_3{\cdot}F^-$ complex anions were produced by electrospraying an $\sim 0.1 \times 10^{-3}$ M mixture solution of NaF salt in water/acetonitrile (1/3 ratio) in an environment containing a relatively high concentration of carbon dioxide vapor. The generation of other halide clusters was slightly different: aqueous solutions of KX (X = Cl, Br, I) salt with a concentration of $\sim 0.4 \times 10^{-3}$ M were bubbled by a flow of carbon dioxide for 30 minutes, and then mixed in acetonitrile at a volume ratio of 1 : 3. The carbonic acid–halide anions were generated by electrospraying the solutions into vacuum, while the sample cone was exposed to a CO_2 flow passing through a bubbler of water.

All produced anions were guided by two RF-only quadruples into a 3D cryogenic ion trap, where they were accumulated and cooled down at $\sim$20 K. The cold anions were then pulsed out into the extraction zone of the TOF mass spectrometer at 10 Hz, and the desired anions were mass-selected, decelerated, and intercepted by a probe laser beam in the photodetachment zone of the magnetic-bottle photoelectron analyzer. In the current experiment, a 157 nm F_2 laser and a 193 nm ArF excimer laser were used to detach electrons from target complex anions containing fluoride and the other halides, respectively. The lasers were operated at a 20 Hz repetition rate with the anion beam turned off at alternating laser shots, enabling shot-by-shot background subtraction. Using a 5.2 m-long magnetic-bottle electron flight tube, the TOF distribution of the detached electrons was analyzed and then converted into a kinetic energy spectrum after calibration with the known data of I^-, $Cu(CN)_2^-$ and $Au(CN)_2^-$. The electron binding energies (eBEs) of anions were determined by subtracting the electron kinetic energies from the photon energies used.

Theoretical methods

To study the structures, energetics, and spectral features of the complex anions $H_2CO_3{\cdot}X^-$ (X = F, Cl, Br, and I) and their corresponding neutrals, CCSD(T) calculations were performed. The aug-cc-pVTZ-PP basis set with the Stuttgart–Köln MCDHF RSC ECP (10 and 28 core electrons, respectively)[41] was used for Br and I atoms, while the standard all-electron aug-cc-pVTZ basis set[42] was adopted for all other atoms. Both basis sets were obtained from the EMSL Basis Set Exchange.[43,44] All geometry optimizations were conducted without any initial symmetry constraints, and vibrational frequency analyses were carried out to ensure the true minima were obtained and to calculate the zero-point energy (ZPE) corrections. For comparison, multi-reference configuration interaction (MRCI) calculations were also performed for each $H_2CO_3{\cdot}X^-$ (X = Cl, Br, and I) anion and the corresponding neutral molecule using the optimized geometries obtained at the CCSD(T) or the CASSCF(6,8) (for anion) and CASSCF(5,8) (for neutral) levels, respectively. Such active spaces were chosen to include all the halogen np electrons among the eight valence orbitals (three p orbitals for halogen, two unoccupied p orbitals for carbon, and three unoccupied p orbitals for three oxygens).

For the complex anions, the vertical detachment energy (VDE) was calculated as the energy difference between the neutral and the corresponding anion, both at the optimized anion's geometry, while the adiabatic detachment energy (ADE) was determined as the energy difference between the neutral and anion, each at its own optimized geometry including ZPE corrections. In addition, to assess the spin–orbit (SO) coupling effect for open-shell neutral radicals, the Breit–Pauli operator,[45,46] together with the third-order Douglas–Kroll–Hess scalar relativistic corrections[47] for the X = Br and I complexes, was used in the MRCI calculations with a slightly different basis set, *i.e.*, aug-cc-pVTZ-DK

of the Douglas–Kroll contracted basis set[48] for Br/I atoms and the aug-cc-pVTZ basis set for all other atoms. All the CCSD(T) and MRCI calculations were performed using the MOLPRO 2015.1 software package.[49]

Results and discussion

NIPES spectra

In this work, NIPES combined with an electrospray ionization source is applied, a methodology that has been proven as a powerful experimental technique to probe molecular structures of complex clusters.[50–52] Many efforts were made to challenge the difficulties in the generation of all carbonic acid–halide complexes in order to render a comprehensive comparison of all $H_2CO_3{\cdot}X^-$ (X = F, Cl, Br, and I) NIPE spectra. Fig. 1 shows the low-temperature NIPE spectra of $H_2CO_3{\cdot}X^-$ (X = Cl, Br, and I) photodetached at 193 nm (6.424 eV) and $H_2CO_3{\cdot}F^-$ at 157 nm (7.867 eV). Compared to isolated halide anions, all complex anions have significantly higher electron binding energies (eBEs), indicating that the extra electron is substantially stabilized by H_2CO_3 in the clusters. The NIPE spectrum of $H_2CO_3{\cdot}I^-$ contains two dominant peaks centered at 4.10 and 5.02 eV, respectively. Because of the 0.92 eV energy interval, which is close to the SO splitting of iodine (0.943 eV),[53] the two bands are easily designated as the contributions of $H_2CO_3{\cdot}I(^2P_{3/2})$ and $H_2CO_3{\cdot}I(^2P_{1/2})$. Compared to the NIPE spectrum of the isolated iodide anion (the blue curve in Fig. 1a), each SO splitting peak is broadened presumably due to vibrational excitations occurring in the photodetachment process. Moreover, the lower eBE band of $H_2CO_3{\cdot}I(^2P_{3/2})$ is wider than the $H_2CO_3{\cdot}I(^2P_{1/2})$ band at the higher eBE side. This disparity can be attributed to the further splitting of the $I(^2P_{3/2})$ state due to electrostatic interaction with the close-shell H_2CO_3 at a sufficiently small distance. In Hund's case (a), the $^2P_{3/2}$ state can split into X(1/2) and A(3/2) sub-states, which is determined by the projection (Ω) of the total electronic angular momentum onto the symmetry axis.[37,38,54] However, no splitting occurs for the $^2P_{1/2}$ state, leaving B(1/2) in a unique state.

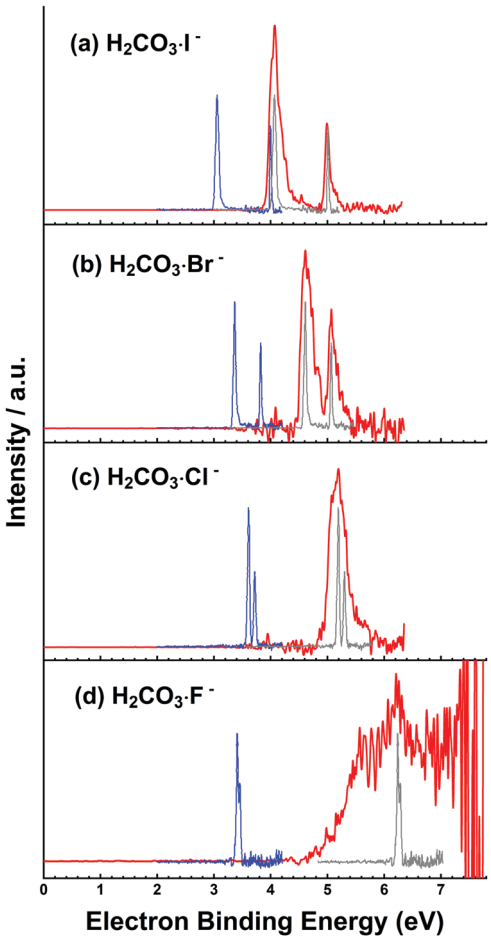

Fig. 1 Low-temperature photoelectron spectra of $H_2CO_3{\cdot}X^-$ (X = Cl, Br, and I) at 193 nm (6.424 eV) and $H_2CO_3{\cdot}F^-$ at 157 nm (7.867 eV). The blue and gray curves are the original and shifted spectra of the corresponding isolated halides, respectively, which are adapted from ref. 53.

Similarly, two distinct peaks were located at 4.61 and 5.07 eV for the $H_2CO_3{\cdot}Br^-$ complex anion, and the 0.46 eV energy gap is also identical to the SO splitting of 0.457 eV for Br ($^2P_{3/2}$ and $^2P_{1/2}$).[53] In the case of the $H_2CO_3{\cdot}Cl^-$ complex anion, only one unresolved wide peak was observed with the center at 5.20 eV, due to the too small SO splitting of Cl (0.109 eV).[53] Thus, consistent assignments are obtained for these three $H_2CO_3{\cdot}X^-$ (X = Cl, Br, and I) complexes, wherein their NIPE spectra have identical patterns to those of the corresponding isolated halide anions with significant blue-shifts in eBEs. This observation strongly suggests that the electron is detached from the halide in the complexes. In other words, the negative charge of the complexes remains in the halide moiety, and no proton transfer occurs during the formation of $H_2CO_3{\cdot}X^-$ (X = Cl, Br, and I). The above conjecture appears consistent with the fact that the PA values of X^- (1395, 1353, and 1315 kJ mol^{-1} for Cl^-, Br^-, and I^-, respectively[55]) are smaller than that of bicarbonate (HCO_3^-, 1490 kJ mol^{-1}),[56] thus hindering proton transfer (PT) from carbonic acid to the halide in the formation of the complex anions, as indicated by the NIPE spectra.

Taking the experimental resolution into account, the vertical detachment energies (VDEs) and the adiabatic detachment energies (ADEs) of the complex anions can be determined from the first peak maximum and onset threshold in the NIPE spectra. Table 1 summarizes the experimental VDEs and ADEs of $H_2CO_3{\cdot}X^-$ (X = Cl, Br, and I), as well as the observable SO splittings. Their close VDE and ADE values for each complex imply that both geometries of neutral and anion are similar. Moreover, the eBE difference (ΔeBE) between the complex anions and the corresponding isolated anions directly reflects the interaction strength between the host neutral molecule and the guest anion.[57] Since apparently different widths exist for the complexes and the isolated halides, ΔVDEs are more reliable to study the binding energies between H_2CO_3 and X^-, *e.g.* 1.58 eV for $H_2CO_3{\cdot}Cl^-$, 1.25 eV for $H_2CO_3{\cdot}Br^-$, and 1.04 eV for $H_2CO_3{\cdot}I^-$, respectively. Along the atomic sequence of X^- (X = Cl, Br, and I), the decreasing ΔVDE value indicates a gradually reduced interaction strength between the halide anion and H_2CO_3, which shows a consistent trend with the respective halide PAs.

Table 1 Theoretical and experimental ADEs, VDEs, and binding energies (BEs) for the $H_2CO_3{\cdot}X^-$ (X = F, Cl, Br, and I) complex anions, as well as the spin–orbit (SO) splittings of the photodetached neutral complexes and isolated halogens

	ADE (eV)			VDE (eV)			BE (eV)		SO Splitting (eV)	
X	Expt.	CCSD(T)	MRCI	Expt.	CCSD(T)	MRCI	Expt.[a]	CCSD(T)	Expt.[b]	MRCI
F	4.72	4.60	—	6.24	6.13	—	2.82	2.63	—(0.051)	—
Cl	4.96	5.33	5.16	5.2	5.67	5.61	1.58	1.56	—(0.109)	0.22
Br	4.52	4.94	4.49	4.61	5.17	4.83	1.25	1.35	0.46(0.457)	0.48
I	3.99	4.50	4.07	4.10	4.65	4.31	1.04	1.12	0.92(0.943)	1.04

[a] The experimental binding energy (BE) is determined as ΔVDE from the isolated halide anions. [b] The experimental SO splitting for complex anions is determined as the energy difference between the $^2P_{3/2}$ and $^2P_{1/2}$ states. The values in the parentheses are the SO splitting values of halogen atoms from the spectra of the isolated halides (from ref. 53).

In contrast to the X = Cl, Br and I cases, the spectrum of $H_2CO_3{\cdot}F^-$ shown in Fig. 1d is markedly different from that of the isolated F^-. An extremely broadened band was observed, spanning the eBE range from 4.5 to 7.6 eV. The whole band can be roughly viewed as consisting of partially resolved sub-bands, centered at ~5.5, 6.2 and ~6.9 eV, respectively. In the region near the photon energy limit at 157 nm, notable oscillations blurred the spectral profile to some extent due to the poor detection efficiency of low kinetic energy electrons and imperfect background subtraction. Apparently, the extraordinarily broadened band of $H_2CO_3{\cdot}F^-$ cannot be attributed to the SO splitting of fluorine as was observed in the other $H_2CO_3{\cdot}X^-$ anions, implying that $H_2CO_3{\cdot}F^-$ might have a different molecular structure from the others. Because F^- has a larger PA (1556 kJ mol^{-1} [55]) than HCO_3^- (1490 kJ mol^{-1} [56]), it is entirely reasonable to assume an intramolecular PT during complex formation that produces the [HOC(O)$O^-\cdots$HF] structure occurs. The complex anion of [HOC(O)$O^-\cdots$HF] deservedly has a similar spectral motif to HCO_3^-,[58,59] however, its experimental spectra are entirely inconsistent. Therefore, high-level quantum chemical calculations and spectral analysis are needed to help illuminate the true origins of the spectral complexity for $H_2CO_3{\cdot}F^-$ (see next sections). In addition, the VDE of 6.24 eV and the ADE of 4.72 eV, derived from the spectrum, yield a 2.5 eV |VDE − ADE| difference for $H_2CO_3{\cdot}F^-$, a difference much larger than those of the other $H_2CO_3{\cdot}X^-$ (X = Cl, Br, and I) complexes, indicative of demonstrable changes regarding its molecular geometry during electron detachment. The obtained ΔVDE of 2.82 eV blueshift from isolated F^- is also the largest among all four complexes.

Optimized structures and energetics

It is well-known that H_2CO_3 has three conformers, namely *cis–cis*, *cis–trans*, and *trans–trans*, suggesting that PT may occur along different geometries with the approach of X^-. Thus, both the reactant and product of PT with [HOC(O)OH$\cdots X^-$] and [HOC(O)$O^-\cdots$HX] structures were initially assumed and checked in geometry optimizations. To our surprise, they eventually converged to a unique optimized one for each type. Moreover, like another diprotic oxyacid, $H_2SO_4{\cdot}X^-$,[30] complex anions with double hydrogen bonds might also be formed with *trans–trans* H_2CO_3, as reported in the previous IR action spectroscopy study of $H_2CO_3{\cdot}F^-$.[27] In this study, we successfully obtained the optimized geometries for multiple $H_2CO_3{\cdot}X^-$ anion isomers at the CCSD(T) level, as shown in Fig. 2. In general, these isomers can be classified into two families, *i.e.*, one with the

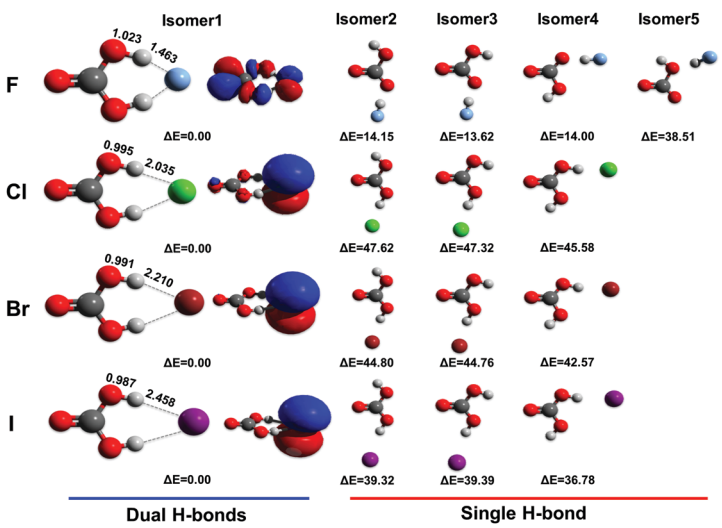

Fig. 2 Optimized geometries and related energies (in kJ mol^{-1}) of isomers for $H_2CO_3{\cdot}X^-$ (X = F, Cl, Br, and I) complex anions, calculated at the CCSD(T)/aug-cc-pVTZ(-PP) level of theory, where the distances of O–H and H$\cdots$X bonds are noted with the unit of Å. The highest occupied molecular orbitals (HOMOs) of Isomer 1 are exhibited as well.

formation of double hydrogen bonds (Isomer1), and the others with single hydrogen bonds (Isomers 2–5). The calculated relative energies of all complex anion isomers after the zero-point energy (ZPE) corrections are also listed in Fig. 2.

For the single hydrogen-bond structures of $H_2CO_3{\cdot}X^-$ (X = Cl, Br, and I), Isomers 2, 3 and 4 are formed when X^- approaches the *cis–cis*, *cis–trans*, *trans–cis* H_2CO_3 conformers, respectively. These isomers have the $[HOC(O)OH\cdots X^-]$ (X = Cl, Br, I) structure, as shown in Fig. 2, while $[HOC(O)O^-\cdots HF]$ is predicted for the $H_2CO_3{\cdot}F^-$ isomers. This change is consistent with the PA sequence of the constituent anions, where $I^- < Br^- < Cl^- < HCO_3^- < F^-$. Due to the fact that isomers 2, 3, and 4 differ only in the conformer of H_2CO_3 (X = Cl, Br, I) (HCO_3 for X = F) and all belong to the binding motif with a single hydrogen-bond, all the isomers have close energies and the geometry of the H_2CO_3 moiety remains intact for the large halide complexes. Of special interest is the observation that the energy sequence of these H_2CO_3 conformers in the complexes is different from those of isolated carbonic acid. At the CCSD(T) level, the *cis–cis* conformer is most stable for carbonic acid itself, while the *cis–trans* and *trans–trans* conformers have higher energies of 6.53 and 40.25 kJ mol^{-1}, respectively. However, under the action of X^- (X = Cl, Br, and I), Isomer 4 in the *cis–trans* conformation is slightly more stable compared to the others (Isomers 2 and 3) owing to the reduced repulsive force between X^- and carbonyl oxygen. Notably, a special isomer 5 was found for the $H_2CO_3{\cdot}F^-$ complex, in which the formed HF molecule is connected to the remaining hydroxyl. Evidently, this isomer can be produced by the subsequent HF migration of Isomer 4, when F^- approaches the *trans*-OH group. That is, the formed HF group of Isomer 4 can further migrate to the other side to produce the $[O_2COH\cdots HF]$ structure. However, as indicated in Fig. 2, this migration is endothermic by $\sim$24 kJ mol^{-1} from Isomer 4.

In Isomer 1, the carbonic acid moiety adopts the C_{2v} structure with a planar *trans–trans* conformation, and two hydrogen bonds are simultaneously formed between two hydroxyl groups and the halide anion, producing a loose six-membered ring structure (Fig. 2). Isomer 1 is the most stable among all anion complex conformers, irrespective of different halide anion types, implying that strong stabilization by dual hydrogen bonds makes the *trans–trans* conformation become the global minimum. Meanwhile, the double hydrogen bond provides an explanation for the significantly higher eBEs observed in experiments. Our present calculations are consistent with the recent study of $H_2CO_3{\cdot}F^-$ by Thomas *et al.*[27] As shown in Fig. 2, all geometries of Isomer 1 for $H_2CO_3{\cdot}X^-$ are very similar, in which both hydroxyl hydrogen atoms remain in the carbonic acid without PT. Taking $H_2CO_3{\cdot}Cl^-$ for example, both O–H bond lengths are slightly increased from 0.963 Å in the isolated carbonic acid to 0.995 Å, while the distance between chloride and the hydroxyl hydrogen atom is 2.035 Å, a typical strong ionic hydrogen bond length of $[O\text{–}H\cdots Cl^-]$. Moreover, along the sequence of $F^- \rightarrow Cl^- \rightarrow Br^- \rightarrow I^-$, the gradually shortened O–H bond length and elongated $X\cdots H$ distance in the complexes are consistent with the charge-induced intensities of X^- indicated by their PA values.

It is worth noting that, for the X = F case, the $H\cdots F$ distance is only 1.463 Å, a significantly shorter length than in the other cases. This strongly implies that two formed H–F bonds in this six-membered ring show evident covalent characteristics. These properties are hypothesized to be essential in causing its different spectral pattern shown in Fig. 1d from that of isolated F^- or the other $H_2CO_3{\cdot}X^-$ (X = Cl, Br, and I) complexes. In addition, Isomers 2–4 of $H_2CO_3{\cdot}X^-$ (X = Cl, Br, and I) are higher in energy than Isomer 1 by $\sim$40 kJ mol^{-1}. These energy differences are close to the isolated single hydrogen bond energy of $O\text{–}H\cdots X$, indicating no significant repulsive interaction between the two hydrogen bonds in Isomer 1. In contrast, Isomers 2–4 of $H_2CO_3{\cdot}F^-$ with a single hydrogen bond are only higher than Isomer 1 by $\sim$14 kJ mol^{-1}. This can be explained considering the shorter $H\cdots F$ distances in Isomer 1 such that the repulsive interaction between two 2p orbitals of fluorine anions naturally enhances the tension of the six-membered ring and reduces its stability. Based on the relative energies of these isomers of $H_2CO_3{\cdot}X^-$, only Isomer 1 is discussed in the following sections according to its dominant thermal distribution.

Using the optimized geometries of Isomer 1 and its associated optimized neutrals (Fig. S1, ESI†), the VDEs and ADEs of $H_2CO_3{\cdot}X^-$ complex anions were calculated at both CCSD(T) and MRCI levels. The SO splitting of the corresponding neutral complex was also calculated at the MRCI level. As indicated in Table 1, a good agreement between the experimental and the calculated data at both CCSD(T) and MRCI levels of theory is achieved. Moreover, the binding energies (BEs) between H_2CO_3 and halide in $H_2CO_3{\cdot}X^-$ can be calculated according to equation (1) including ZPE corrections.

$$BE = E(H_2CO_3) + E(X^-) - E(H_2CO_3{\cdot}X^-) \quad (1)$$

where $E(H_2CO_3)$, $E(X^-)$ and $E(H_2CO_3{\cdot}X^-)$ are the energies of neutral H_2CO_3, the isolated X^- anion, and the complex anion, each at its own optimized geometry with the same conformation. For the $H_2CO_3{\cdot}X^-$ complex anions, the calculated BEs were 2.63, 1.56, 1.35, and 1.12 eV for X = F, Cl, Br, and I, respectively, as listed in Table S1 (ESI†). The variation trend of BEs agrees very well with the experimental ΔVDE values.

Bonding analyses and spectral simulations

As two representative diprotic oxyacids, H_2CO_3 and H_2SO_4 might have similar complex structures with halide anions. A recent investigation,[30] however, revealed an unordinary structure of $[HSO_4^-{\cdot}HF]$ for the sulfuric acid–fluoride complex, in which one $O\text{–}H\cdots F$ hydrogen bond and one $O\cdots H\text{–}F$ hydrogen bond are formed with the approach of F^-, in contrast to $[H_2CO_3{\cdot}F^-]$, where the fluoride anion plays the role of an acceptor for two identical $O\text{–}H\cdots F$ hydrogen bonds (Fig. 2). Certain covalent bond characteristics were suggested for these $H\cdots F$ bonds in $[H_2CO_3{\cdot}F^-]$ to account for their short bond lengths. In order to quantify the chemical interactions along the whole series of $[H_2CO_3{\cdot}X^-]$, we further characterized their binding motifs with the electron density, $\rho(r)$, and charge populations for the $O\text{–}H\cdots X$ bonds of Isomer 1, using the theory of "atoms in molecules (AIM)"[60,61] with the Multiwfn

program[62] (Fig. S2, ESI†). On the electron localization function[63] surfaces of all $H_2CO_3{\cdot}X^-$, electrons along both O–H···X paths are predominantly localized between oxygen and hydrogen atoms, indicative of their covalent characteristics. Meanwhile, the covalent O–H bond strength increases in the sequence of F → Cl → Br → I (Table S2, ESI†), where the X^- anions play the role of a charge inducer. Moreover, natural population analyses (NPAs) confirmed that more than 80% of the extra negative charge resides on halides in this complex anion series (Fig. S3, ESI†). The smooth bond strength change and similar NPA charges for all $H_2CO_3{\cdot}X^-$ complex anions discussed above, nevertheless, appear to contradict the fact that an extraordinarily complicated spectrum is observed for $H_2CO_3{\cdot}X^-$ X = F, as compared to the simple spectra for X = Cl, Br, and I.

Since the highest occupied molecular orbital (HOMO) locates the primarily detached electron of complex anions, Fig. 2 displays the calculated HOMOs of Isomer 1 of $H_2CO_3{\cdot}X^-$. For $H_2CO_3{\cdot}X^-$ (X = Cl, Br, and I), the HOMO is mainly contributed by the p orbital of X^-, thus causing these complex anions to exhibit similar photoelectron spectra to their respective isolated halides. However, to our surprise, the HOMO of $H_2CO_3{\cdot}F^-$ is entirely different from the other carbonic acid–halide anions, even though the four complex anions look similar in the structural binding motif. As shown in Fig. 2, the HOMO is primarily localized on the carbonyl oxygen of $H_2CO_3{\cdot}F^-$, while F^- also makes a significant contribution. Therefore, the NIPE spectrum of this complex anion should have a different pattern from that of the isolated F^-.

As discussed above, the NIPE spectra of $H_2CO_3{\cdot}X^-$ (X = Cl, Br, and I) show similar spectral patterns to those of the isolated halides, dominantly contributed by two SO states with the lower eBE band X($^2P_{3/2}$) further splitting into two sub-states of X(1/2) and A(3/2),[37,38,54] while the $^2P_{1/2}$ state remains as the unique B(1/2) state. Thus, a simple spectral simulation of density of states (DOS) based on the theoretically generalized Koopman's theorem[64,65] was applied to analyze the NIPE spectra of $H_2CO_3{\cdot}X^-$ (X = Cl, Br, and I). In addition, the Franck–Condon (FC) factor calculations were also performed using the ezSpectrum program[66] to simulate the accompanied vibrational structures in the spectra. To facilitate the comparisons, Fig. 3 stands as an example to show the experimental, DOS and FC factor simulated spectra of $H_2CO_3{\cdot}Br^-$ based on Isomer 1.

Apparently, major spectral patterns were clearly simulated by the DOS method; the three sub-states of X, A and B are marked with sticks in Fig. 3a. However, the B peak predicted by the DOS method is inconsistent with the experimental spectrum. Our previous study of $[F{\cdots}H{\cdots}F]^-$ anions[67] indicated to us that the spectral complexity can also be derived from vibrational excitations. Using the optimized geometries of the anion and neutral $H_2CO_3{\cdot}Br$ complex (Fig. 2 and Fig. S1, ESI†), their relative energies, and vibrational frequencies, the predominant FC transitions were calculated and noted with colour sticks in Fig. 3b. Apparently, vertical transitions are dominant for the three sub-states due to the similar geometries of both the neutral and anion. The FC simulated spectrum is

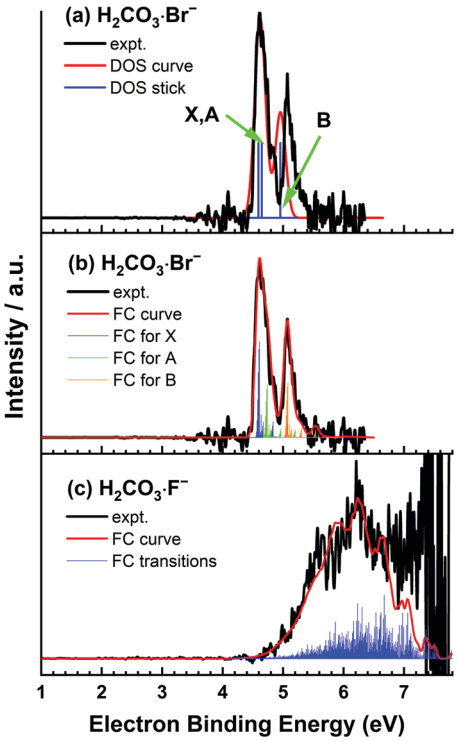

Fig. 3 Density of states (DOS) (a), Franck–Condon (FC) factor simulated spectra of $H_2CO_3{\cdot}Br^-$ (b), and $H_2CO_3{\cdot}F^-$ (c) with H_2CO_3 in *trans–trans* conformation. The corresponding experimental spectra are also exhibited for comparison.

extremely consistent with the experimental spectrum. Encouraged by the good agreement between the FC simulated and experimental spectra, the FC factor calculations were also used to simulate the complicated and distinctive spectrum of $H_2CO_3{\cdot}F^-$ in order to clarify its contributors.

In contrast to the relatively simple spectra of other carbonic acid–halide anions, a gently rising edge is observed at the onset region of the broad band for $H_2CO_3{\cdot}F^-$, covering an eBE range of 4.5–5.5 eV. In addition, large noise blurred the actual spectral signals in the highest eBE region, as shown in Fig. 2. Thus, the spectral feature at lower eBEs becomes the key criterion to perform FC simulations. It is especially worth noting that in the neutral $H_2CO_3{\cdot}F$ complex (Fig. S1, ESI†), two types of hydrogen bonds are clearly identified as O–H···F and O···H–F, respectively, in which the fluorine atom acts as both an acceptor and donor of two hydrogen bonds. In contrast, in the anionic state, F^- only plays the role of a proton-acceptor for the double hydrogen bonds in $H_2CO_3{\cdot}F^-$, as shown in Fig. 2. Such a dramatic anion → neutral geometry change associated with hydrogen relocation not only results in its extremely small photodetachment cross section per energy interval, but it also produces a large difference between VDE and ADE, as indicated in Table 1. Moreover, extensive vibrational modes are expected to be excited in photodetachment based on this significant geometry rearrangement. Such a complicated spectrum of $H_2CO_3{\cdot}F^-$ might be expected from its distinctive delocalized HOMO, as shown in Fig. 2.

As shown in Fig. 3c, the FC simulated spectrum is consistent with the experimental data, especially in the rising edge at lower eBEs. Indeed, massive vibrational transitions are involved and six dominant peaks centered at 5.55, 5.86, 6.25, 6.64, 7.01 and 7.43 eV, respectively, emerge from the simulation, yielding a simulated spectrum that is in overall good agreement with the experimental profile. The two simulated bands at 7.01 and 7.43 eV, however, have much less intensity compared to the experiments, most likely due to other detachment channels kicking in. In addition, for $H_2CO_3{\cdot}F^-$, Isomers 2–4 have a slightly higher energy relative than Isomer 1 by 14.15, 13.62 and 14.00 kJ mol^{-1}, respectively. Thus, they could possibly survive from an electrospray ionization source and contribute to the experimental spectra, even though their thermal populations based on the Boltzmann distribution are only $\sim$0.5% at 298 K and even less in the low-temperature trap. To rule out their contributions, the FC factor calculations and the spectral simulations were also carried out for these isomers. As shown in Fig. S4 and S5 (ESI†), the FC simulated spectra of Isomers 2, 3 and 5 are obviously very different from the experimental data, indicating no contributions from these isomers (an almost 90° rotation of HF around HCO_3 in the anion $\rightarrow$ neutral transition causes diminished FCFs for Isomer 4). At this stage, we have identified the structure of all $H_2CO_3{\cdot}X^-$ complexes to be dual hydrogen bonded Isomer 1 without PT during complex anion formation based on good agreements between observed and simulated spectra as well as between measured and calculated ADEs and VDEs.

How to describe diprotic oxyacid–halide complexes: PA or pK_a?

Of special interest is what is the most determinant factor in stabilizing carbonic acid–halide complexes, which is also the key point to unveil different geometries of $H_2CO_3{\cdot}X^-$ and $H_2SO_4{\cdot}X^-$.[30] It is well-known that PA plays a pivotal role in determining hydrogen-bonding structures in related complex systems. As a thermodynamic parameter, PA can successfully describe the proton attraction ability of an isolated base in the gas phase, such as in the complex formation between hexafluoroisopropanol (HFIP) and halogen anions X^- (X = F, Cl, Br, and I).[68] We must emphasize that the correlation between the PA of the anion and the hydrogen-bonding strength is true for the system with a single hydrogen bond, *e.g.* Isomers 2, 3 and 4 (including Isomer 5) of $H_2CO_3{\cdot}X^-$ (X = F, Cl, Br, and I). However, in a complicated structure like Isomer 1 that involves the formation of two hydrogen bonds, the prediction based on purely the PA sequence is incorrect because of the lack of proton-transfer from the carbonic acid moiety to the fluoride anion, as discussed above. A similar phenomenon also existed in the $H_2SO_4{\cdot}X^-$ (X = F, Cl, Br, and I) system.[30] From the PA perspective, all X^- anions could readily attract a proton from sulfuric acid due to their higher PAs than HSO_4^-. However, a recent investigation confirmed the opposite conclusions,[30] such that no PT occurs between H_2SO_4 and X^- (X = Cl, Br, and I), and that the true complex structure is $[H_2SO_4{\cdot}X^-]$ with two O–H$\cdots$X$^-$ hydrogen bonds between H_2SO_4 and X^-. Therefore, PAs of the constituent bases cannot correctly predict the chemistry for proton bound systems that involve the formation of multiple hydrogen bonds.

In contrast, the acid dissociation constant (pK_a) has always been used to reflect the ability of acids to release a proton in aqueous solutions, as shown in the following definition (2):

$$HA(aq) + H_2O(l) \rightarrow H_3O^+(aq) + A^-(aq)$$

$$pK_a = -\log_{10}([H_3O^+]{\cdot}[A^-]/[HA]) \quad (2)$$

The competition between the proton acceptors of A^- and oxygen atoms of water is taken into account in pK_a, while in the gas phase, only one proton attraction of a molecule is included in the PA definition. For a diprotic oxyacid in the *trans–trans* conformation, like Isomer 1 of $H_2CO_3{\cdot}X^-$, two identical hydroxyls interact with X^- simultaneously when approached by anions. This synergistic interaction is evidently different from the isolated attraction elucidated in the PA definition, resulting in its invalidity. Notably, this complicated interaction among two hydroxyls and X^- is similar to some extent to the situation of diprotic oxyacid in aqueous solution, in which X^- plays the same role as an oxygen atom of water. Consequently, the pK_a might be able to properly predict the occurrence of proton-transfer in the diprotic oxyacid–halide complex anions. Table 2 summarizes the pK_a values of all acids involved in this work, *i.e.* H_2CO_3, H_2SO_4, HF, HCl, HBr and HI, as well as the PA data of the related species, HCO_3^-, HSO_4^-, F^-, Cl^-, Br^- and I^-.

It is very exciting that a qualitative consistency was captured for these acids in order to explain the perplexing phenomena of proton transfer in their most stable isomers with two hydrogen bonds in accordance with their pK_a trend. Because the pK_a values of all HX (X = F, Cl, Br, and I) acids are smaller (more acidic) than that of H_2CO_3, no proton transfer occurs in the formation of Isomer 1 of $H_2CO_3{\cdot}X^-$. In contrast, it is feasible to transfer one proton from H_2SO_4 hydroxyl to F^- due to the lower pK_a value of sulfuric acid, although the proton transfer is not allowed in the other halide anion cases because their pK_a values are lower than that of H_2SO_4. Therefore, compared with PA, pK_a can better describe the most stable hydrogen bonding structures of diprotic oxyacid–halide anions.

In addition, it is meaningful to assess the BE between acid and halide anions based on their PA values. With the PA decrease along the $F^- \rightarrow Cl^- \rightarrow Br^- \rightarrow I^-$ sequence, the BE value of $H_2CO_3{\cdot}X^-$ was reduced monotonically, as mentioned above, owing to the weak double hydrogen bonding interactions. As a result, the formation of $H_2CO_3{\cdot}X^-$ complex anions

Table 2 pK_a values of the acids, H_2CO_3, H_2SO_4 and HX (X = F, Cl, Br, and I), together with the PAs (in kJ mol^{-1}) of the corresponding anions

	H_2CO_3	H_2SO_4	HF	HCl	HBr	HI
pK_a[a]	6.35	−3.0	3.17	−5.9	−8.8	−9.5
PA[b]	1490	1295	1556	1395	1353	1315

[a] The pK_a values of H_2CO_3, H_2SO_4 and HF are from ref. 69, and those of HCl, HBr and HI are from ref. 70. [b] The corresponding anions are HCO_3^-, HSO_4^-, and X^- (X = F, Cl, Br, and I), respectively. The PA value of HCO_3^- is from ref. 56, and the others are from ref. 55.

is more and more difficult for larger halides. To verify this conclusion, we performed *ab initio* calculations of the Gibbs free energy for the formation of Isomer 1 $H_2CO_3{\cdot}X^-$ complexes. As listed in Table S3 (ESI†), the $\Delta_fG_{298.15}$ values increase progressively in the atomic sequence. Notably, negative $\Delta_fG_{298.15}$ values were determined for $H_2CO_3{\cdot}X^-$ (X = F, Cl, and Br), but a positive value was obtained for $\Delta_fG_{298.15}$ of $H_2CO_3{\cdot}I^-$. Thus, from the thermodynamic perspective, $H_2CO_3{\cdot}X^-$ (X = F → Cl → Br → I) complex anions are increasingly difficult to generate at room temperature. Fortunately, the exceedingly soft electrospray ionization source, together with the rapid cooling in the cryogenic trap employed in our experiments allowed us to successfully retain these weakly bound species.

Conclusions

Holistic $H_2CO_3{\cdot}X^-$ (X = F, Cl, Br, and I) complex anions have been successfully observed in the present experiments, indicative of the efficient stabilization of carbonic acid by halide anions. We further carried out a joint experimental and theoretical study on the NIPE spectra of $H_2CO_3{\cdot}X^-$. For the X = Cl, Br and I cases, the observed spectral patterns are similar to those of the respective X^- but shifted to the high electron binding energy side. For $H_2CO_3{\cdot}F^-$, an extremely wide band was recorded, spanning the eBE range from 4.5 to 7.6 eV. A special six-membered ring structure is suggested for the most stable isomer 1 of $H_2CO_3{\cdot}X^-$, in which the carbonic acid moiety adopts a planar *trans–trans* conformation. Notably, two identical O–H···X hydrogen bonds are formed with the approach of X^-, which is believed to be the key for the formation and stabilization of carbonic acid–halide complexes. Upon electron detachment, only marginal geometry changes are observed for the X = Cl, Br, and I complexes. In contrast, a significant geometric rearrangement associated with electron-detached hydrogen atom relocation from carbonic acid to fluoride is unravelled, manifested by the appearance of the extraordinary complexity in the $H_2CO_3{\cdot}F^-$ spectrum.

Special attention has been paid to determining the most important factor in stabilizing hydrogen bonding structures of carbonic acid–halide anions. It appears that PA can be generally used to decide the proton location in proton bound systems that involve only one hydrogen bond, but such a prediction cannot convey correct structural binding motifs for diprotic oxyacid–halide complexes, *e.g.* $H_2CO_3{\cdot}X^-$ and $H_2SO_4{\cdot}X^-$, where multiple hydrogen bonding interactions exist. To our delight, we found a perfect consistency between the pK_a trend of acids and their most stable hydrogen bonding structures, strongly suggesting that pK_a values are a valid parameter to predict proton locations and binding motifs for the stabilization of diprotic oxyacids by halide anions.

Conflicts of interest

There are no conflicts to declare.

Acknowledgements

This work was supported by the U.S. Department of Energy (DOE), Office of Basic Energy Sciences, Division of Chemical Sciences, Geosciences, and Biosciences, and performed using EMSL, a national scientific user facility sponsored by the DOE's Office of Biological and Environmental Research and located at the Pacific Northwest National Laboratory, which is operated by Battelle Memorial Institute for the DOE. The theoretical calculations were conducted on the EMSL Cascade Supercomputer. The financial support of the National Natural Science Foundation of China (No. 21873089) and the National Key Research and Development Program of China (No. 2016YFF0200502) is gratefully acknowledged too.

Notes and references

1 A. J. Andersson, F. T. Mackenzie and A. Lerman, *Global Biogeochem. Cycles*, 2006, **20**, GB1S92.
2 N. Stolte and D. Pan, *J. Phys. Chem. Lett.*, 2019, **10**, 5135–5141.
3 G. Strazzulla, J. R. Brucato, G. Cimino and M. E. Palumbo, *Planet. Space Sci.*, 1996, **44**, 1447–1450.
4 W. Hage, K. R. Liedl, A. Hallbrucker and E. Mayer, *Science*, 1998, **279**, 1332–1335.
5 M. L. Delitsky and A. L. Lane, *J. Geophys. Res.: Planets*, 1998, **103**, 31391–31403.
6 I. Kurtz, J. Kraut, V. Ornekian and M. K. Nguyen, *Am. J. Physiol.: Renal Physiol.*, 2008, **294**, F1009–F1031.
7 D. Aminov, D. Pines, P. M. Kiefer, S. Daschakraborty, J. T. Hynes and E. Pines, *Proc. Natl. Acad. Sci. U. S. A.*, 2019, **116**, 20837–20843.
8 B. Jönsson, G. Karlström, H. Wennerström and B. Roos, *Chem. Phys. Lett.*, 1976, **41**, 317–320.
9 S. A. de Marothy, *Int. J. Quantum Chem.*, 2013, **113**, 2306–2311.
10 S. Ghoshal and M. K. Hazra, *J. Phys. Chem. A*, 2014, **118**, 2385–2392.
11 S. Ghoshal and M. K. Hazra, *RSC Adv.*, 2015, **5**, 17623–17635.
12 J. K. Terlouw, C. B. Lebrilla and H. Schwarz, *Angew. Chem., Int. Ed. Engl.*, 1987, **26**, 354–355.
13 T. Mori, K. Suma, Y. Sumiyoshi and Y. Endo, *J. Chem. Phys.*, 2009, **130**, 204308.
14 J. R. Brucato, M. E. Palumbo and G. Strazzulla, *Icarus*, 1997, **125**, 135–144.
15 P. Gerakines, M. H. Moore and R. L. Hudson, *Astron. Astrophys.*, 2000, **357**, 793–800.
16 W. Zheng and R. I. Kaiser, *Chem. Phys. Lett.*, 2007, **450**, 55–60.
17 C. R. Wu, D. Judge, B. M. Cheng, T. S. Yih, C. Lee and W. Ip, *J. Geophys. Res.: Planets*, 2003, **108**, 5032.
18 M. Garozzo, D. Fulvio, O. Gomis, M. Palumbo and G. Strazzulla, *Science*, 2008, **56**, 1300–1308.
19 W. Hage, A. Hallbrucker and E. Mayer, *J. Am. Chem. Soc.*, 1993, **115**, 8427–8431.
20 M. Moore and R. Khanna, *Spectrochim. Acta, Part A*, 1991, **47**, 255–262.

21 G. Bucher and W. Sander, *Science*, 2014, **346**, 544–545.
22 J. Bernard, R. G. Huber, K. R. Liedl, H. Grothe and T. Loerting, *J. Am. Chem. Soc.*, 2013, **135**, 7732–7737.
23 K. Winkel, W. Hage, T. Loerting, S. L. Price and E. Mayer, *J. Am. Chem. Soc.*, 2007, **129**, 13863–13871.
24 C. Mitterdorfer, J. Bernard, F. Klauser, K. Winkel, I. Kohl, K. R. Liedl, H. Grothe, E. Mayer and T. Loerting, *J. Raman Spectrosc.*, 2012, **43**, 108–115.
25 H. P. Reisenauer, J. P. Wagner and P. R. Schreiner, *Angew. Chem., Int. Ed.*, 2014, **53**, 11766–11771.
26 K. Adamczyk, M. Premont-Schwarz, D. Pines, E. Pines and E. T. Nibbering, *Science*, 2009, **326**, 1690–1694.
27 D. A. Thomas, E. Mucha, M. Lettow, G. Meijer, M. Rossi and G. von Helden, *J. Am. Chem. Soc.*, 2019, **141**, 5815–5823.
28 P. Ayotte, S. B. Nielsen, G. H. Weddle, M. A. Johnson and S. S. Xantheas, *J. Phys. Chem. A*, 1999, **103**, 10665–10669.
29 W. H. Robertson and M. A. Johnson, *Annu. Rev. Phys. Chem.*, 2003, **54**, 173–213.
30 G. L. Hou and X. B. Wang, *J. Phys. Chem. Lett.*, 2019, **10**, 6714–6719.
31 G. H. Gardenier, J. R. Roscioli and M. A. Johnson, *J. Phys. Chem. A*, 2008, **112**, 12022–12026.
32 I. Alata, M. Broquier, C. Dedonder-Lardeux, C. Jouvet, M. Kim, W. Y. Sohn, S.-S. Kim, H. Kang, M. Schuetz, A. Patzer and O. Dopfer, *J. Chem. Phys.*, 2011, **134**, 074307.
33 T. C. Cheng, B. Bandyopadhyay, J. D. Mosley and M. A. Duncan, *J. Am. Chem. Soc.*, 2012, **134**, 13046–13055.
34 D. Bing, T. Hamashima, C.-W. Tsai, A. Fujii and J.-L. Kuo, *Chem. Phys.*, 2013, **421**, 1–9.
35 T. I. Yacovitch, N. Heine, C. Brieger, T. Wende, C. Hock, D. M. Neumark and K. R. Asmis, *J. Chem. Phys.*, 2012, **136**, 241102.
36 G.-L. Hou, X.-B. Wang and M. Valiev, *J. Am. Chem. Soc.*, 2017, **139**, 11321–11324.
37 Y. X. Zhao, C. C. Arnold and D. M. Neumark, *J. Chem. Soc., Faraday Trans.*, 1993, **89**, 1449–1456.
38 D. W. Arnold, S. E. Bradforth, E. H. Kim and D. M. Neumark, *J. Chem. Phys.*, 1995, **102**, 3493–3509.
39 E. Garand, T. Wende, D. J. Goebbert, R. Bergmann, G. Meijer, D. M. Neumark and K. R. Asmis, *J. Am. Chem. Soc.*, 2010, **132**, 849–856.
40 X. B. Wang and L. S. Wang, *Rev. Sci. Instrum.*, 2008, **79**, 073108.
41 R. Krishnan, J. S. Binkley, R. Seeger and J. A. Pople, *J. Chem. Phys.*, 1980, **72**, 650–654.
42 R. A. Kendall, T. H. Dunning Jr and R. J. Harrison, *J. Chem. Phys.*, 1992, **96**, 6796–6806.
43 K. L. Schuchardt, B. T. Didier, T. Elsethagen, L. Sun, V. Gurumoorthi, J. Chase, J. Li and T. L. Windus, *J. Chem. Inf. Model.*, 2007, **47**, 1045–1052.
44 D. Feller, *J. Comput. Chem.*, 1996, **17**, 1571–1586.
45 D. G. Fedorov, S. Koseki, M. W. Schmidt and M. S. Gordon, *Int. Rev. Phys. Chem.*, 2003, **22**, 551–592.
46 D. G. Fedorov and M. S. Gordon, *J. Chem. Phys.*, 2000, **112**, 5611–5623.
47 T. Nakajima and K. Hirao, *J. Chem. Phys.*, 2000, **113**, 7786–7789.
48 W. A. De Jong, R. J. Harrison and D. A. Dixon, *J. Chem. Phys.*, 2001, **114**, 48–53.
49 P. J. K. H.-J. Werner, F. R. Manby, M. Schütz, P. Celani, G. Knizia, T. Korona, R. Lindh, A. Mitrushenkov, G. Rauhut, T. B. Adler, R. D. Amos, A. Bernhardsson, A. Berning, D. L. Cooper, M. J. O. Deegan, A. J. Dobbyn, F. Eckert, E. Goll, C. Hampel, A. Hesselmann, G. Hetzer, T. Hrenar, G. Jansen, C. Köppl, Y. Liu, A. W. Lloyd, R. A. Mata, A. J. May, S. J. McNicholas, W. Meyer, M. E. Mura, A. Nicklass, P. Palmieri, K. Pflüger, R. Pitzer, M. Reiher, T. Shiozaki, H. Stoll, A. J. Stone, R. Tarroni, T. Thorsteinsson, M. Wang and A. Wolf, *MOLPRO, version 2015.1, a package of ab initio programs*, 2015.
50 G.-L. Hou, J. Zhang, M. Valiev and X.-B. Wang, *Phys. Chem. Chem. Phys.*, 2017, **19**, 10676–10684.
51 Q. Yuan, X.-T. Kong, G.-L. Hou, L. Jiang and X.-B. Wang, *Faraday Discuss.*, 2019, **217**, 383–395.
52 G.-L. Hou, W. Lin, S. Deng, J. Zhang, W.-J. Zheng, F. Paesani and X.-B. Wang, *J. Phys. Chem. Lett.*, 2013, **4**, 779–785.
53 M. Cheng, Y. Feng, Y. Du, Q. Zhu, W. Zheng, G. Czakó and J. M. Bowman, *J. Chem. Phys.*, 2011, **134**, 191102.
54 H. Haberland, *Z. Phys. A: At. Nucl.*, 1982, **307**, 35–39.
55 E. P. J. Linstrom and W. J. Mallard, National Institute of Standards and Technology, Gaithersburg, MD, retrieved March 15, 2020, p. 20899, DOI: 10.18434/T4D303.
56 R. R. Squires, *Int. J. Mass Spectrom. Ion Processes*, 1992, **117**, 565–600.
57 J. Zhang, B. Zhou, Z.-R. Sun and X.-B. Wang, *Phys. Chem. Chem. Phys.*, 2015, **17**, 3131–3141.
58 X. B. Wang and S. S. Xantheas, *J. Phys. Chem. Lett.*, 2011, **2**, 1204–1210.
59 H. Wen, G. L. Hou, Y. R. Liu, X. B. Wang and W. Huang, *Phys. Chem. Chem. Phys.*, 2016, **18**, 17470–17482.
60 R. F. Bader, *Chem. – Eur. J.*, 2006, **12**, 7769–7772.
61 R. F. Bader and H. Essén, *J. Chem. Phys.*, 1984, **80**, 1943–1960.
62 T. Lu and F. Chen, *J. Comput. Chem.*, 2012, **33**, 580–592.
63 R. W. Taft, I. Koppel, R. Topsom and F. Anvia, *J. Am. Chem. Soc.*, 1990, **112**, 2047–2052.
64 B. N. Plakhutin and E. R. Davidson, *J. Phys. Chem. A*, 2009, **113**, 12386–12395.
65 D. J. Tozer and N. C. Handy, *J. Chem. Phys.*, 1998, **109**, 10180–10189.
66 V. A. Mozhayskiy and A. I. Krylov, *ezSpectrum*, http://iopenshell.usc.edu/downloads.
67 G.-L. Hou, X.-B. Wang, A. B. McCoy and W. T. Borden, *J. Phys. Chem. A*, 2017, **121**, 7895–7902.
68 L. Wang, Q. Yuan, W. Cao, J. Han, X. Zhou, S. Liu and X.-B. Wang, *J. Phys. Chem. A*, 2020, **124**, 2036–2045.
69 D. C. Harris, *Quantitative Chemical Analysis*, W. H. Freeman, New York, 8th International ed., 2010; pp. AP12–AP14.
70 A. Trummal, L. Lipping, I. Kaljurand, I. A. Koppel and I. Leito, *J. Phys. Chem. A*, 2016, **120**, 3663–3669.